mater.scichina.com link.springer.com

Sci China Mater 2025, 68(7): 2337–2346
https://doi.org/10.1007/s40843-025-3389-3

PtNi nanoparticles with rich hydroxyl species as efficient catalysts for the electrochemical hydrogen evolution reaction in seawater

Wen-Ying Zhao[1†], Xiong Yang[1†], Yu-Xuan Xiao[2*], Fei Yu[1], Ge Tian[1], Ling Shen[1], Yi Lu[1], Wei Geng[1], Si-Ming Wu[1], Jie Ying[2], Ion Tiginyanu[3], Kenneth I. Ozoemena[4] and Xiao-Yu Yang[1,5*]

ABSTRACT **Adsorption and corrosion caused by Cl^- are the main reasons for the low performance of Pt-based catalysts for the hydrogen evolution reaction (HER) in seawater. Although the introduction of hydroxyl species is an ideal approach to enhance HER kinetics and resist harmful Cl^-, achieving this goal in Pt-based catalysts is challenging. In this study, we developed a high-temperature reduction process to generate PtNi alloy particles that contain Ni vacancies (Lewis acid sites) that participate in transforming lattice hydroxyls to dissociative hydroxyls on Ni layered double hydroxides (Ni-LDH). The hydroxyls in Ni-LDH bind with Lewis acid active sites to form hydroxyl rich species, a process which enhances the hydrophilicity of PtNi/Ni-LDH to promote water adsorption and enhance resistance to Cl^- absorption. Owing to these properties, PtNi/Ni-LDH exhibits superior performance as an electrocatalyst for the HER in alkaline natural seawater as reflected by a low overpotential of 19 mV to drive a current density of 10 mA cm^{-2}, a low Tafel slope of 31 mV dec^{-1}, and an only slightly elevated overpotential after 100 h of operation. This study throws light on the development of new strategies for the design of high-performance catalysts for hydrogen production by electrolytic seawater splitting.**

Keywords: platinum, surface hydroxyl species, heterojunction interface, seawater hydrogen evolution

INTRODUCTION

Electrocatalytic seawater splitting is a promising strategy for low-cost and large-scale hydrogen production [1–5]. Studies have demonstrated that problems associated with microorganism fouling, and Ca^{2+} and Mg^{2+} precipitation that limit the efficiency of the cathodic hydrogen evolution reaction (HER) can be mitigated by using alkaline seawater [6–8]. Also, efforts have shown that platinum (Pt) is one of the best catalysts for the HER due to its optimal hydrogen adsorption/desorption energy [9–11]. Furthermore, it has been found that alloying with other transition metals, especially nickel (Ni), enhances the HER performance of Pt-based electrocatalysts by altering its electronic state [12–14]. In spite of these advances, the HER performance and durability of PtNi catalysts in alkaline seawater are still unsatisfactory [15–18]. Factors that contribute to their low HER performance include the unfavorable water dissociation process ($H_2O \rightarrow H^* + OH^*$) promoted by Pt [19–21], and poisoning ($M + Cl^- \rightarrow MCl_{ads} + e^-$, M = metal) and subsequent corrosion ($MCl_{ads} + Cl^- \rightarrow MCl_x^-$; $MCl_x + OH^- \rightarrow M(OH)_x + Cl^-$) caused by the high concentration of Cl^- in seawater [22,23].

One approach to circumventing these limitations of Pt/Ni catalysts is to introduce hydrophilic hydroxyl species onto the Pt surface, which both accelerates water dissociation rate and facilitates water adsorption, thereby lessening competitive Cl^- adsorption [24]. Nevertheless, creating a high density of hydroxyls on Pt is challenging because of the absence of Lewis acid active sites that promote hydroxyl attachment [25–27]. Benefitting from the presence of adsorbed hydroxyl bound to its coordinately unsaturated edge active sites, highly hydrophilic layered double hydroxide (LDH) can be integrated with Pt to enhance the water dissociation process [28–32]. However, the presence of inert basal planes of Ni-LDH limits the number of hydroxyl species that can be introduced [33,34].

In the study described below, a new co-reduction method has been developed to generate a highly efficient HER catalyst. In this catalyst, denoted as PtNi/Ni-LDH, PtNi nanoparticles are anchored on Ni-LDH enriched with surface hydroxyl species, which are generated during high-temperature reduction. The presence of the hydroxyl species leads to significant elevation of the rate of water dissociation and effective mitigation of surface Cl^- adsorption. Consequently, PtNi/Ni-LDH displays exceptional performance and durability as a catalyst for the HER in alkaline natural seawater.

RESULTS AND DISCUSSION

The process for the formation of PtNi/Ni-LDH is depicted schematically in Fig. 1a. In the route, Ni-LDH having a hexagonal nanosheet morphology is synthesized and then used as a substrate to support Pt precursors. When treated with H_2/Ar at

[1] State Key Laboratory of Silicate Materials for Architectures & State Key Laboratory of Advanced Technology for Materials Synthesis and Processing & School of Chemistry, Chemical Engineering and Life Sciences & Laoshan Laboratory & School of Materials Science and Engineering & International School of Materials Science and Engineering, Wuhan University of Technology, Wuhan 430070, China
[2] School of Chemical Engineering and Technology, Sun Yat-sen University, Zhuhai 519082, China
[3] National Center for Materials Study and Testing, Technical University of Moldova, Chisinau 2004, Republic of Moldova
[4] Molecular Sciences Institute, School of Chemistry, University of the Witwatersrand, Johannesburg 2050, the Republic of South Africa
[5] National Energy Key Laboratory for New Hydrogen-Ammonia Energy Technologies, Foshan Xianhu Laboratory, Foshan 528200, China
† Equally contributed to this work.
* Corresponding author (email: xiaoyx63@mail.sysu.edu.cn; xyyang@whut.edu.cn)

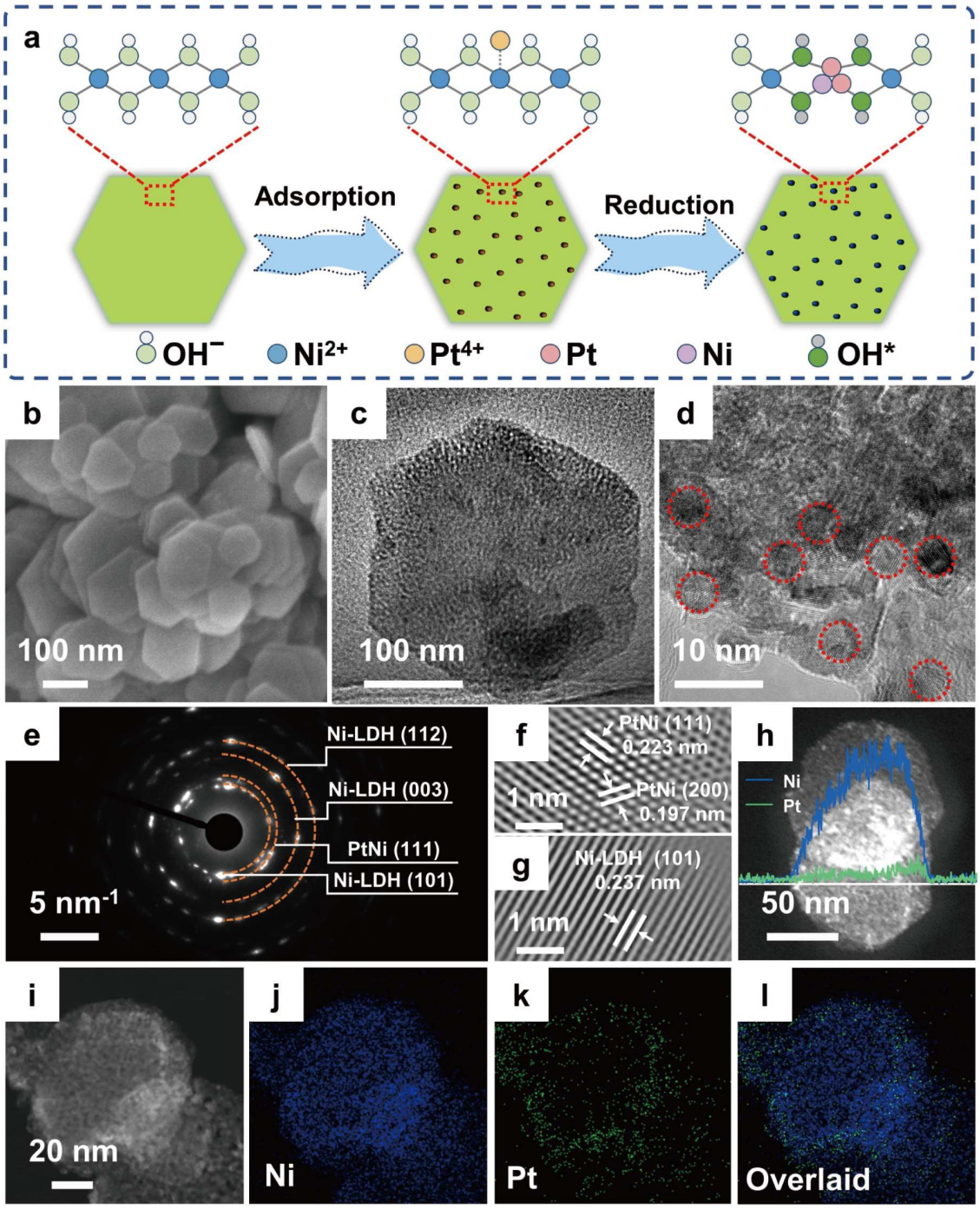

Figure 1 (a) Schematic presentation of the route for the synthesis of PtNi/Ni-LDH. (b) SEM, (c) low and (d) high magnification TEM images of PtNi/Ni-LDH. (e) SAED pattern corresponding to Fig. 1d. IFT patterns of (f) PtNi and (g) Ni-LDH in Fig. 1d. (h) HAADF-STEM image guided EDS line scanning profile. (i) HAADF-STEM image of another region. EDS maps of (j) Ni, (k) Pt, and (l) overlaid color maps of PtNi/Ni-LDH.

200 °C, the interaction of Pt precursors and Ni-LDH facilitated the alloy of Pt and Ni during the reduction process, leading to the leaking of Ni^{2+} from Ni-LDH and simultaneously leaving Ni vacancies in Ni-LDH that serve as Lewis acid centers to bond with dissociative hydroxyls to form hydroxyl species [35,36].

Scanning electron microscopy (SEM) and transmission electron microscopy (TEM) were conducted to ascertain the morphology of PtNi/Ni-LDH. The SEM image in Fig. 1b shows that as-synthesized PtNi/Ni-LDH has a homogeneous two-dimensional (2D) hexagonal nanosheet morphology. Analysis of the corresponding TEM image (Fig. 1c) indicates that the nanosheets have an overall lateral size of ca. 200 nm and that some with a diameter of ca. 5 nm support PtNi alloy particles (Fig. 1d). The selected area electron diffraction (SAED) profile of PtNi/Ni-LDH contains a set of diffraction rings assigned to the (101), (003) and (112) facets of Ni-LDH, and the (111) facets of PtNi alloy (Fig. 1e). Notably, inverse Fourier transformation (IFT) images of the PtNi nanoparticle (Fig. 1f) and nanosheets

(Fig. 1g) show the existence of lattice fringes of 0.223, 0.197 and 0.237 nm, reflecting (111) and (200) facets of PtNi alloys, and (101) facets corresponding to Ni-LDH, respectively. The X-ray energy dispersive profile (EDS) of PtNi/Ni-LDH (guided by the high-angle annular dark-field scanning transmission electron microscopy (HAADF-STEM) image, contains a relatively strong signal for Ni and a relatively weak signal for Pt (Fig. 1h). These observations are in accord with the results of inductively coupled plasma atomic emission spectrometry (ICP-AES) (Table S1). Moreover, the results of EDS elemental mapping indicate that the nanosheets in PtNi/Ni-LDH contain a homogeneous distribution of Pt and Ni (Fig. 1i–l). Notably, Pt tends to be distributed at the edge positions of the nanosheets due to the higher intrinsic edge activity of 2D Ni-LDH, which provides more adsorption sites for the Pt precursor (H_2PtCl_6). This facilitates the synergistic interaction between PtNi alloy and Ni-LDH, thereby enhancing the HER catalytic performance of PtNi/Ni-LDH [37,38]. The combined results presented above illustrate that PtNi alloy is supported on the Ni-LDH nanosheets as synthesized PtNi/Ni-LDH.

Data for a detailed structural characterization of PtNi/Ni-LDH were collected and compared to those arising from the corresponding analysis of independently synthesized PtNi and Ni-LDH (see Fig. S1 for SEM images of Ni-LDH and PtNi). X-ray diffraction (XRD) studies were conducted first to characterize the crystalline structures of the materials. As the profiles in Fig. 2a show, XRD peaks of PtNi/Ni-LDH match well with those of PtNi and Ni-LDH, indicating PtNi alloy becomes well integrated with Ni-LDH during the annealing/reduction process. Notably, when the Ni-LDH was thermally treated in the same condition, no metallic Ni peaks were observed until the temperature was increased to 300 °C (Fig. S2), which clearly

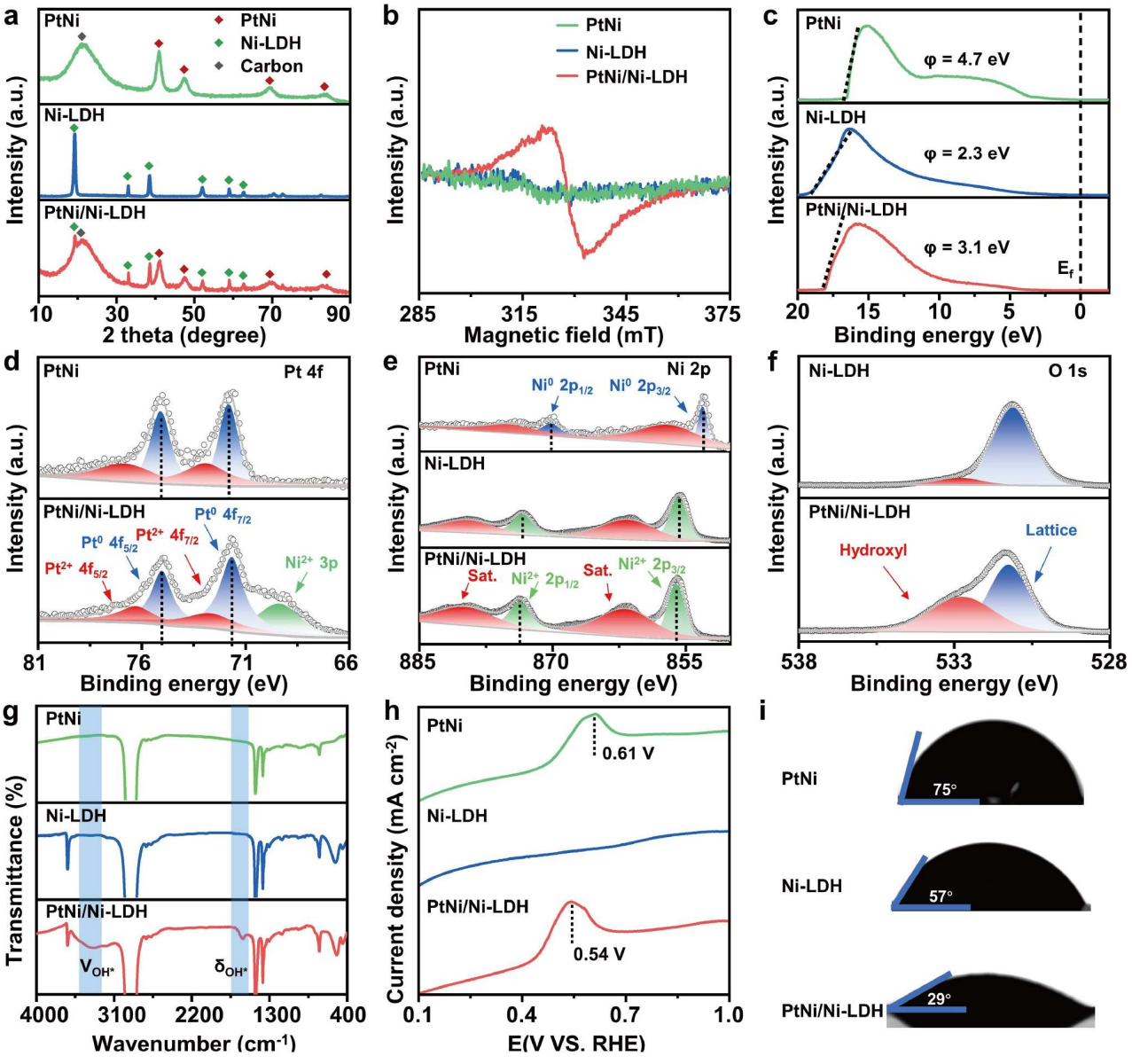

Figure 2 (a) XRD patterns, (b) ESR spectra and (c) UPS spectra of PtNi, Ni-LDH and PtNi/Ni-LDH. XPS spectra and binding energies of (d) Pt 4f for PtNi and PtNi/Ni-LDH, (e) Ni 2p for PtNi, Ni-LDH and PtNi/Ni-LDH, and (f) O 1s for Ni-LDH and PtNi/Ni-LDH. (g) FT-IR spectra, (h) CO-stripping curves in CO-saturated alkaline simulated seawater and (i) water contact angles of the PtNi, Ni-LDH and PtNi/Ni-LDH.

demonstrates the interaction between Pt precursors and Ni-LDH could lower the reductive thermodynamics of Ni that facilitates the leaking of Ni^{2+} from Ni-LDH and thus the formation of Ni vacancies. The results of electron spin resonance (ESR) studies indicate that a much stronger single Lorentzian line signal is present in the spectrum of PtNi/Ni-LDH as compared to those of PtNi and Ni-LDH (Fig. 2b). This observation suggests that PtNi/Ni-LDH has a higher unpaired electron content as a likely result of Ni vacancies in PtNi/Ni-LDH [39]. The peak at ~310 cm^{-1} in the Raman spectrum (Fig. S3) corresponds to the lattice vibration of E-type Ni-OH in the support Ni-LDH, whereas the peak at ~450 cm^{-1} is attributed to the bending vibration of Ni–O in the support Ni-LDH [40]. Compared with Ni-LDH, the bond strength of Ni–O in PtNi/Ni-LDH decreases, which can be ascribed to the presence of Ni vacancies in PtNi/Ni-LDH. The work functions (Φ) of PtNi/Ni-LDH, PtNi and Ni-LDH, which correspond to energies required to move a valence electron from the surface of a solid to infinity, were determined by using ultraviolet photoelectron spectroscopy (UPS). Specifically, smaller Φ values correspond to smaller energy barriers for electron transfer at surfaces of the materials [41]. As shown in Fig. 2c, the trend in the Φ values (PtNi (4.7 eV) > PtNi/Ni-LDH (3.1 eV) > Ni-LDH (2.1 eV)) suggests that the electrons are transferred from Ni-LDH to metals in PtNi/Ni-LDH.

The results of X-ray photoelectron spectroscopy (XPS) studies provided information about the electronic states of surface elements in PtNi/Ni-LDH. Peak fitting analysis of the Pt 4f XPS spectra (Fig. 2d, Table S2) reveals that the Pt^0 $4f_{7/2}$ peaks of this material exhibit negative shifts compared to those of PtNi. This finding indicates that electron transfer occurs from Ni-LDH to PtNi, which is in accordance with the UPS results. Moreover, the Ni $2p_{3/2}$ binding energy of PtNi/Ni-LDH exhibits a positive shift compared to that of PtNi (Fig. 2e), further evidencing the occurrence of electron transfer from Ni-LDH to PtNi. A comparison of O 1s signals for PtNi/Ni-LDH and Ni-LDH indicates that the electrons transfer from Ni-LDH to PtNi originates from O atoms (Fig. 2f). Notably, analysis of the O 1s signals shows that a much higher content of hydroxyl species exists in PtNi/Ni-LDH [42].

Fourier transform infrared (FT-IR) spectroscopy was conducted to ascertain information about the hydroxyl species content of PtNi/Ni-LDH. In these experiments, they were subjected to vacuum drying and then dispersed in nujol to avoid spectral interference of adsorbed H_2O. In contrast to those of PtNi and Ni-LDH, the FT-IR spectrum (Fig. 2g) of PtNi/Ni-LDH contains significant peaks at 3380 and 1612 cm^{-1}, which correspond to the stretching and bending vibrations of hydroxyl groups. Moreover, the presence of peaks at 3637 cm^{-1} corresponding to OH^- stretching vibrations in the spectra of both Ni-LDH and PtNi/Ni-LDH, demonstrates that Ni-LDH in PtNi/Ni-LDH is maintained during annealing [43,44]. CO-stripping curves were generated to evaluate the difficulty of forming hydroxyl species on surfaces of the catalytic materials [45,46]. Specifically, we reasoned that the absorbed hydroxyl species would facilitate CO-stripping and reduce the oxidation potential for CO pre-adsorbed on the surface of the catalysts [47]. As shown in Fig. 2h, PtNi/Ni-LDH (0.54 V) has a lower CO-stripping potential than that of PtNi (0.61 V), indicating that the former material has a greater tendency to form hydroxyl species on its surface. Accordingly, benefiting from the abundance of surface hydroxyl species, PtNi/Ni-LDH has a higher hydrophilicity than those of PtNi and Ni-LDH (Fig. 2i). This property should enhance both the HER activity of PtNi/Ni-LDH in seawater by accelerating the water dissociation rate, and the electrochemical stability of the material by facilitating adsorption of H_2O relative to that of Cl^- [48,49].

The HER performances of PtNi/Ni-LDH in alkaline water (1 M KOH), alkaline simulated seawater (1 M KOH + 3.5 wt.% NaCl) and alkaline natural seawater (1 M KOH + natural seawater) were determined using PtNi/Ni-LDH containing different compositions (PtNi/Ni-LDH with a Pt:Ni ratio of ca. 1:4, PtNi/Ni-LDH-1 with a Pt:Ni ratio of ca. 1:10 and PtNi/Ni-LDH-3 with a Pt:Ni ratio of ca. 1:3, ICP-AES results; see Figs S4, S5 for their structural characterizations). The results show that PtNi/Ni-LDH exhibits higher catalytic performances in both alkaline water and alkaline simulated seawater than those of PtNi/Ni-LDH-1 and PtNi/Ni-LDH-3. This conclusion is based on the observed higher current densities (Fig. S6a–c), smaller overpotentials to drive a current density of 10 mA cm^{-2} (η_{10}) (Fig. S6d, e, f), higher turnover frequency (TOF) values (Fig. S7), and smaller Tafel slopes (Fig. S8). The higher HER activity of PtNi/Ni-LDH is ascribed to its lower charge transfer resistance than those of PtNi/Ni-LDH-1 and PtNi/Ni-LDH-3, as is evidenced by electrochemical impedance spectroscopy (EIS) results (Fig. S9).

The HER performance of PtNi/Ni-LDH was compared to those of PtNi and commercial Pt/C. The data (Fig. 3a, d, g) clearly show that the activities of these catalysts follow the sequence PtNi/Ni-LDH > PtNi > commercial Pt/C in alkaline water, alkaline simulated seawater and alkaline natural seawater. Specifically, PtNi/Ni-LDH displays remarkable HER activities with η_{10} values of only 21 mV in alkaline water (Fig. S10a), 20 mV in alkaline simulated seawater (Fig. S10b) and 19 mV in alkaline natural seawater (Fig. S10c), values that are much lower than those of commercial Pt/C and PtNi. Moreover, PtNi/Ni-LDH exhibits the highest TOF values (Fig. 3b, e, h) in alkaline water (2.35 s^{-1}, Fig. S11a), alkaline simulated seawater (2.27 s^{-1}, Fig. S11b) and alkaline natural seawater (2.53 s^{-1}, Fig. S11c), which are three-fold higher than those of commercial Pt/C in alkaline water and alkaline simulated seawater.

To gain information about the mechanism of the HER catalyzed by PtNi/Ni-LDH, Tafel slopes were acquired by fitting experimental data using the Butler-Volmer equation (Fig. 3c, f, i). PtNi/Ni-LDH displays Tafel slopes of 34, 33 and 31 mV dec^{-1} in alkaline water, alkaline simulated seawater and alkaline natural seawater, respectively, which are much smaller than those of commercial Pt/C and PtNi. Owing to the presence of abundant surface hydroxyls species that accelerate water dissociation, the Tafel step ($2Pt\text{-}H \rightarrow H_2 + 2Pt$) is the rate-determining step in the HER promoted by PtNi/Ni-LDH, while the Heyrovsky step is rate limiting in the process catalyzed by commercial Pt/C and PtNi. Notably, a comparison of overpotential and Tafel slopes indicates that the HER performance of PtNi/Ni-LDH in both alkaline water (Fig. 3j, Table S3) and alkaline seawater (Fig. 3k, Table S4) is superior to those of previously reported electrocatalysts. EIS was carried out to investigate the interface charge transfer in PtNi/Ni-LDH. In this electrocatalyst, Ni vacancies serve as hole-trapping centers in PtNi/Ni-LDH, which facilitate the efficient separation of electron-hole pairs, reduce charge-transfer resistance (R_{ct}) and enhance bulk conductivity (as shown in Fig. S12), thus synergistically boosting the overall electrocatalytic performance. Model photoelectrolytic water devices were assembled using PtNi/Ni-LDH, PtNi and com-

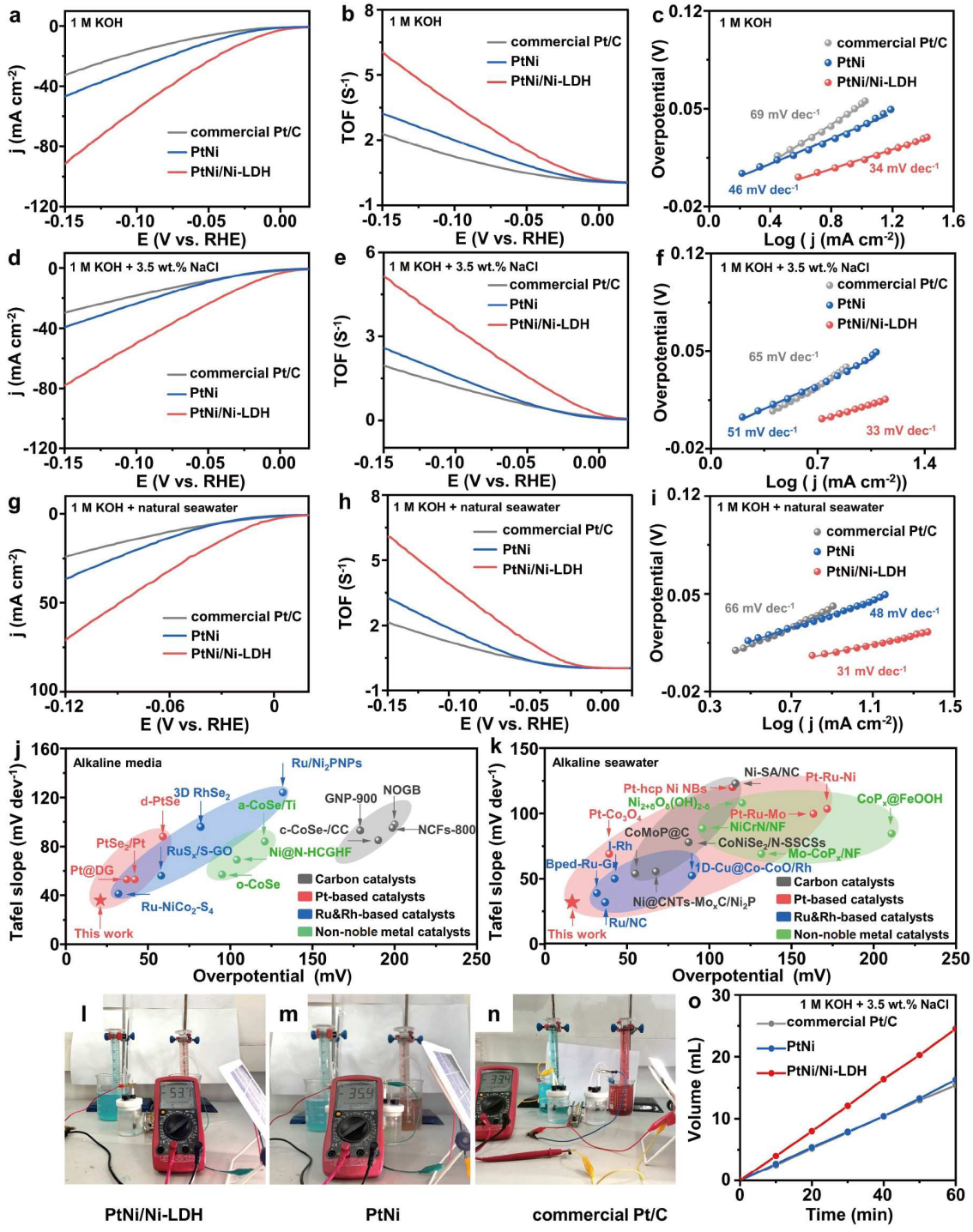

Figure 3 Respective HER polarization curves, calculated TOF curves and Tafel slopes of commercial Pt/C, PtNi and PtNi/Ni-LDH in (a–c) alkaline water, (d–f) alkaline simulated seawater and (g–i) alkaline natural seawater. Performance of PtNi/Ni-LDH in comparison to other catalysts towards the HER in (j) alkaline water and (k) alkaline seawater. Photos of the solar-cell-driven HER devices employing (l) PtNi/Ni-LDH, (m) PtNi and (n) commercial Pt/C as cathodes. (o) Collected H_2 volume (dots) by the solar-cell-driven devices and the theoretical gas volume (lines) for the commercial Pt/C, PtNi and PtNi/Ni-LDH based devices.

mercial Pt/C as cathodes, commercial RuO_2 as the anode and a commercial Si solar cell. The solar-cell driven HER performances of these devices were evaluated in alkaline simulated seawater. Under simulated sunlight, the system using PtNi/Ni-LDH as the cathode achieved a working current of 53.7 mA (Fig. 3l), which is higher than that of devices utilizing PtNi (35.4 mA, Fig. 3m) and commercial Pt/C (33.4 mA, Fig. 3n) as cathodes. In addition, the hydrogen production rate of the PtNi/Ni-LDH||RuO_2 based photoelectrolytic system is 0.018 mmol min^{-1}, which is significantly higher than that of the related PtNi||RuO_2 (0.012 mmol min^{-1}) and commercial Pt/C||RuO_2 (0.011 mmol min^{-1}) based systems (Fig. 3o, Fig. S13). As

the data in Table S5 show, the solar-to-hydrogen (STH) conversion efficiency of the device using PtNi/Ni-LDH as a cathode is 16.3%, a value that surpasses those inherent to PtNi (10.9%) and commercial Pt/C (10.3%) based systems. Furthermore, the Faradaic efficiencies of the photoelectrolytic system containing PtNi/Ni-LDH||RuO_2, PtNi||RuO_2 and commercial Pt/C||RuO_2 were all nearly 100%, and each system maintains a H_2 to O_2 volume ratio of 2:1.

The durability of PtNi/Ni-LDH during its participation in electrocatalysis was evaluated using the chronopotentiometry technique. As shown in Fig. 4a, PtNi/Ni-LDH exhibits superior durability with only 10 mV decline in η_{10} value after 100 h of the chronoamperometric test in alkaline water. This value is much smaller than those of PtNi and commercial Pt/C (a 112 and 87 mV decline in η_{10} value after 20 h, respectively). In alkaline simulated seawater and alkaline natural seawater, PtNi and commercial Pt/C undergo dramatic 184, 177 mV and 163, 142 mV declines, respectively, within 20 h in the chronoamperometric test (Fig. 4b, c), which is ascribed to adsorption and corrosion by Cl^- in the electrolyte. PtNi/Ni-LDH, however, shows only 44 and 25 mV decline in η_{10} value after 100 h testing. These results definitively illustrate the high electrocatalytic durability of PtNi/Ni-LDH in alkaline water, alkaline simulated seawater and alkaline natural water as a result of the abundance of surface hydroxyls species.

Studies were conducted to examine if PtNi/Ni-LDH undergoes structural changes during catalysis of the HER in alkaline simulated seawater. The XRD profile of PtNi/Ni-LDH following

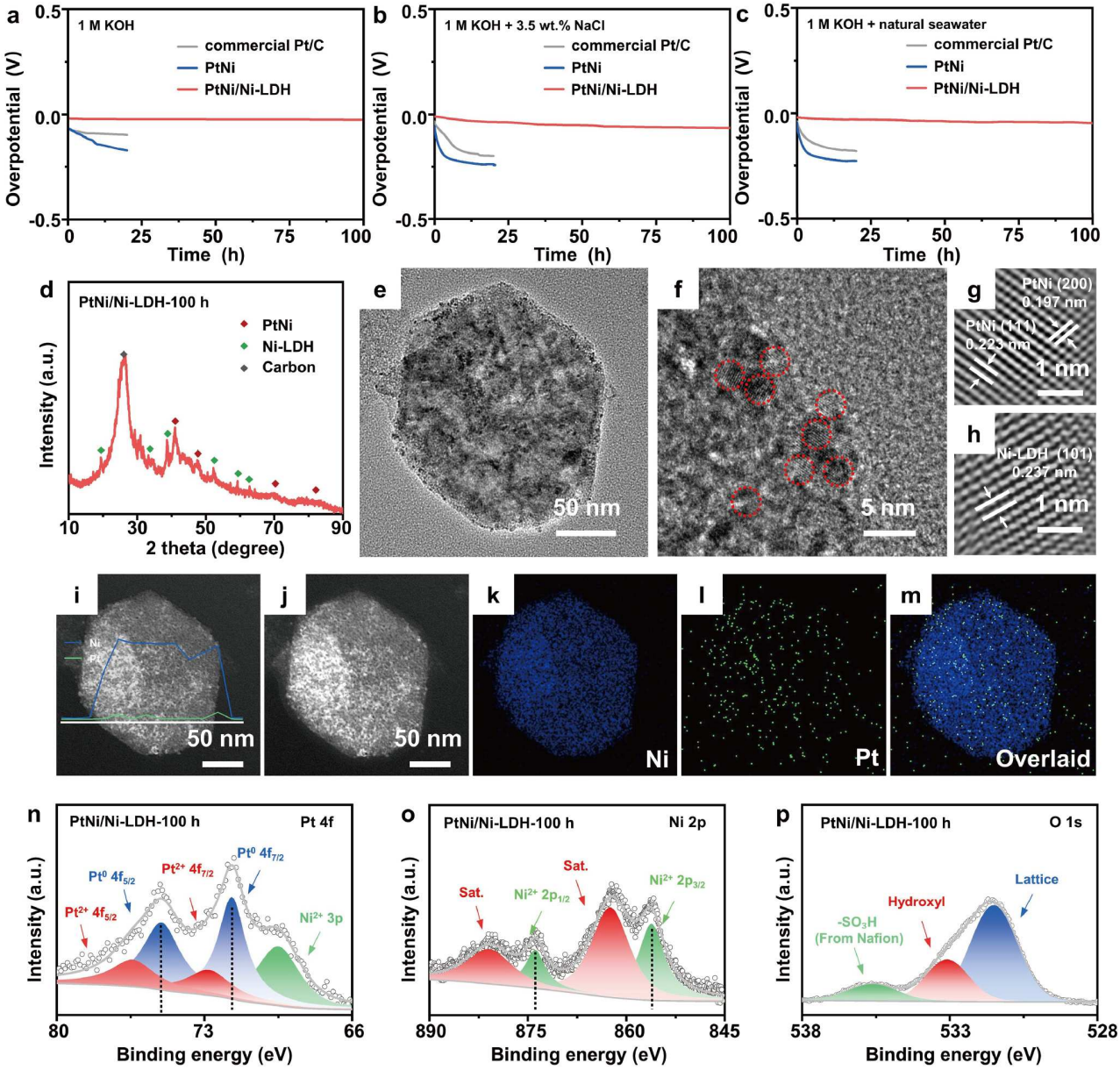

Figure 4 Chronopotentiometry of commercial Pt/C, PtNi and PtNi/Ni-LDH at a current density of 10 mA cm^{-2} in (a) alkaline water, (b) alkaline simulated seawater and (c) alkaline natural seawater. (d) XRD pattern, (e) low and (f) high magnification TEM images, lattice fringes of (g) PtNi and (h) Ni-LDH. (i) STEM-EDS line scanning profile. (j) HAADF-STEM image and EDX mapping images of (k) Ni, (l) Pt and (m) overlaid color mapping. XPS spectra and binding energies of (n) Pt 4f, (o) Ni 2p, and (p) O 1s for PtNi/Ni-LDH after 100 h of durability test in alkaline simulate seawater.

the HER for 100 h (Fig. 4d) contains characteristic peaks for PtNi alloy and Ni-LDH, indicating that no electrochemically induced reconstruction occurs. Moreover, the 2D hexagonal nanosheet morphology of the Ni-LDH substrate (Fig. 4e) and the nanoparticle morphology of the PtNi alloy (Fig. 4f) are retained after the 100 h of the chronoamperometric test. Furthermore, the lattice fringes of PtNi and Ni-LDH (Fig. 4g, h), as well as the homogeneously distributed Pt signals throughout the 2D hexagon structure (Fig. 4i–m) remain the same as before the HER. Notably, the Pt content in PtNi/Ni-LDH-100 h (Fig. 4m) exhibits a significant decrease compared to PtNi/Ni-LDH (Fig. 1l), as evidenced by ICP-AES (Table S1) analysis (from 17% to 14%), indicating a slight dissolution of Pt species during the 100-h stability test. The XPS spectra of PtNi/Ni-LDH-100 h show that the binding energies of Pt^0 $4f_{7/2}$ (Fig. 4n, Table S2) and Ni^{2+} $2p_{3/2}$ (Fig. 4o, Table S2) match those of PtNi/Ni-LDH, and the O 1s (Fig. 4p) spectra retain the hydroxyl oxygen signal, indicating that PtNi/Ni-LDH has high structural stability.

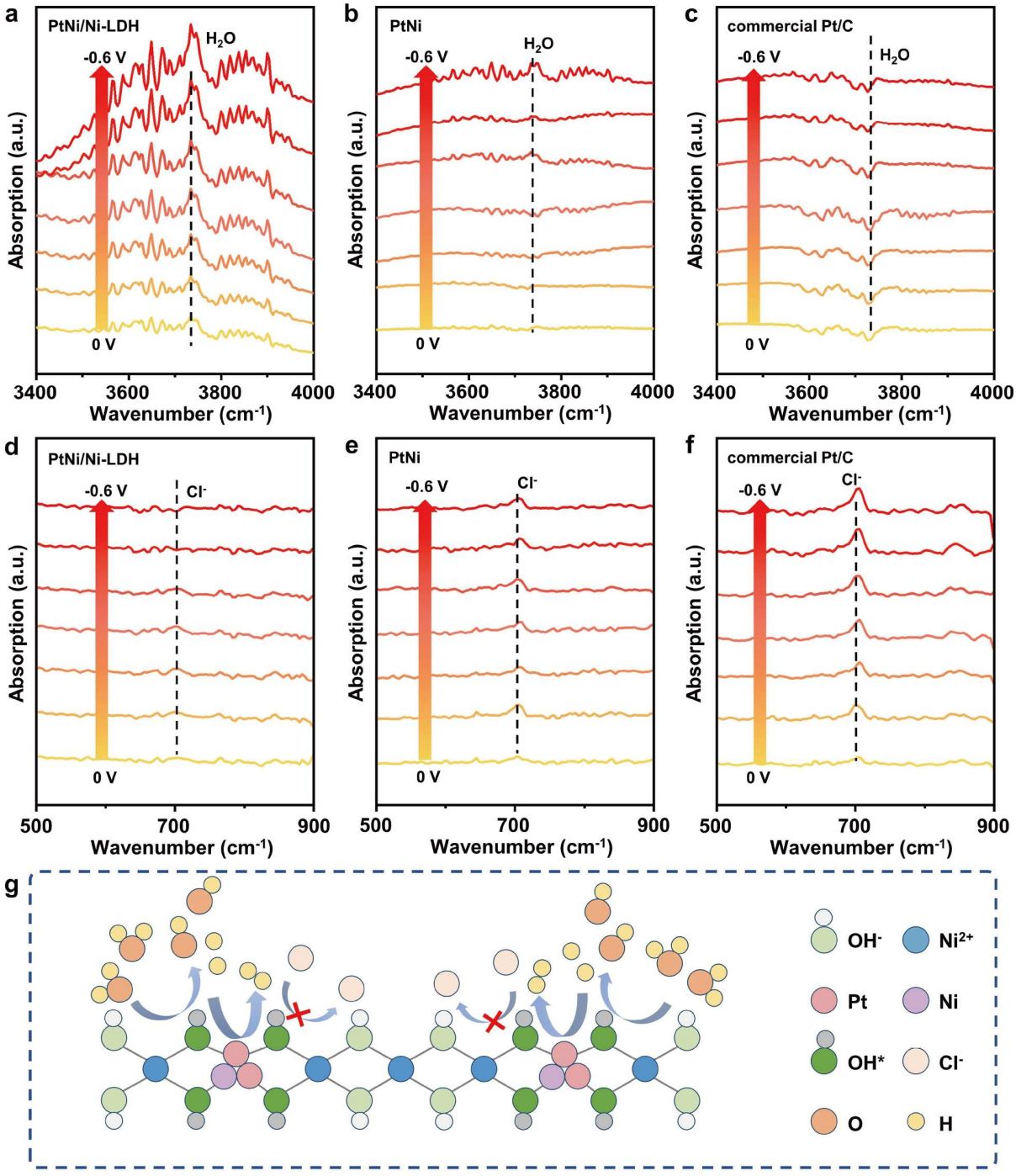

Figure 5 *In situ* FT-IR spectra of the (a, d) PtNi/Ni-LDH, (b, e) PtNi and (c, f) commercial Pt/C at various applied potentials. (g) A schematic diagram of the interaction mechanisms among surface hydroxyl groups, water molecules, and Cl^-.

Finally, an *in-situ* FT-IR spectroscopy investigation was performed to assess reasons for the superior electrocatalytic performance of PtNi/Ni-LDH. In the spectrum of PtNi/Ni-LDH (Fig. 5a), the H_2O adsorption peak at 3710 cm^{-1} become more intense with the increases in the applied potential than those in the spectra of PtNi (Fig. 5b) and commercial PtC (Fig. 5c), demonstrating that the former catalyst engages in a much more facile water dissociation process [50,51]. Moreover, when the applied potential is increased the Cl^- adsorption peak at 710 cm^{-1} in the FT-IR spectrum of PtNi/Ni-LDH (Fig. 5d) does not increase as strongly as those in the spectra of PtNi (Fig. 5e) and commercial Pt/C (Fig. 5f) [52,53]. The schematic diagram in Fig. 5g shows the interaction mechanisms among surface hydroxyl groups, water molecules, and Cl^- in PtNi/Ni-LDH. The surface hydroxyl species in PtNi/Ni-LDH improve its hydrophilicity to accelerate the Volmer step (H_2O adsorption/dissociation), and provide more H* for the HER reaction, thereby enhancing its HER activity. Meanwhile, the adsorption of water molecules reduces the adsorption of Cl^- through competitive adsorption, effectively mitigating chloride-induced corrosion and preserving structural integrity during seawater electrolysis.

CONCLUSIONS

In this study, we developed a two-step method for the synthesis of the novel electrocatalyst PtNi/Ni-LDH, which contains hydroxyl species between PtNi particles and Ni-LDH. In addition, we demonstrated that the presence of the hydroxyl species enhances the hydrophilicity of PtNi/Ni-LDH, leading to enhanced water adsorption and dissociation, simultaneously increasing the resistance to adsorption of Cl^- in the alkaline simulated seawater and alkaline natural seawater. As a result of these properties, PtNi/Ni-LDH exhibits superior activity and durability in its catalysis of the HER in alkaline water, alkaline simulated seawater and alkaline natural seawater. This study sheds light on a new strategy to design of high-performance catalysts for hydrogen production by seawater splitting.

Received 12 March 2025; accepted 4 May 2025; published online 29 May 2025

1 Liu W, Niu X, Tang J, *et al.* Energy-efficient anodic reactions for sustainable hydrogen production via water electrolysis. Chem Synth, 2023, 3: 44
2 Yu Y, Xu H, Xiong X, *et al.* Ultra-thin RuIr alloy as durable electrocatalyst for seawater hydrogen evolution reaction. Small, 2024, 20: 2405784
3 Yang X, Xiao YX, Yu F, *et al.* Direct synthesis of PtNi coated with Ni_3B for efficient electrochemical hydrogen evolution from seawater. Chem Commun, 2025, 61: 760–763
4 Yang X, Xiao YX, Chen JB, *et al.* Surface controllable anchoring of Cu onto nanostructured PtNi for efficient electrochemical hydrogen evolution from seawater. Sci China Mater, 2023, 66: 3887–3894
5 Xiao YX, Ying J, Liu HW, *et al.* Pt–C interactions in carbon-supported Pt-based electrocatalysts. Front Chem Sci Eng, 2023, 17: 1677–1697
6 Dresp S, Dionigi F, Loos S, *et al.* Direct electrolytic splitting of seawater: activity, selectivity, degradation, and recovery studied from the molecular catalyst structure to the electrolyzer cell level. Adv Energy Mater, 2018, 8: 1800338
7 Dresp S, Dionigi F, Klingenhof M, *et al.* Direct electrolytic splitting of seawater: opportunities and challenges. ACS Energy Lett, 2019, 4: 933–942
8 Zhao L, Zhou S, Lv Z, *et al.* Anti-precipitation molecular metal chalcogenide complexes modification for efficient direct alkaline seawater splitting at the large current density. Appl Catal B-Environ, 2023, 338: 122996
9 Luo F, Guo L, Xie Y, *et al.* Iridium nanorods as a robust and stable bifunctional electrocatalyst for pH-universal water splitting. Appl Catal B-Environ, 2020, 279: 119394
10 Ma T, Cao H, Li S, *et al.* Crystalline lattice-confined atomic Pt in metal carbides to match electronic structures and hydrogen evolution behaviors of platinum. Adv Mater, 2022, 34: 2206368
11 Liu L, Wang Y, Zhao Y, *et al.* Ultrahigh Pt-mass-activity hydrogen evolution catalyst electrodeposited from bulk Pt. Adv Funct Mater, 2022, 32: 2112207
12 Li Y, Miao YC, Yang C, *et al.* Ir nanodots decorated Ni_3Fe nanoparticles for boosting electrocatalytic water splitting. Chem Eng J, 2023, 451: 138548
13 Xiao Y, Liu D, Yang J, *et al.* Controllable reconstruction of β-Bi_2O_3/$Bi_2O_2CO_3$ composite for highly efficient and durable electrochemical CO_2 conversion. Nano Lett, 2025, 25: 6548–6555
14 Kim MS, Tran DT, Nguyen TH, *et al.* Ni single atoms and Ni phosphate clusters synergistically triggered surface-functionalized MoS_2 nanosheets for high-performance freshwater and seawater electrolysis. Energy & Environ Mater, 2022, 5: 1340–1349
15 Yu F, Xiao YX, Chen JB, *et al.* Interfacial sulfur-sensitization of PtNi nanoalloy for efficient electrocatalytic hydrogen production in alkaline simulated seawater. Chem Mater, 2023, 35: 8529–8539
16 Jin H, Wang X, Tang C, *et al.* Stable and highly efficient hydrogen evolution from seawater enabled by an unsaturated nickel surface nitride. Adv Mater, 2021, 33: 2007508
17 Xiao YX, Ying J, Tian G, *et al.* Hierarchically fractal PtPdCu sponges and their directed mass- and electron-transfer effects. Nano Lett, 2021, 21: 7870–7878
18 Xiao YX, Ying J, Tian G, *et al.* PtPd hollow nanocubes with enhanced alloy effect and active facets for efficient methanol oxidation reaction. Chem Commun, 2021, 57: 986–989
19 Xiang K, Song Z, Wu D, *et al.* Bifunctional Pt–Co_3O_4 electrocatalysts for simultaneous generation of hydrogen and formate via energy-saving alkaline seawater/methanol co-electrolysis. J Mater Chem A, 2021, 9: 6316–6324
20 Xiao YX, Ying J, Chen JB, *et al.* Confined ultrafine Pt in porous carbon fibers and their N-enhanced heavy d-π effect. Chem Mater, 2022, 34: 3705–3714
21 Xiao YX, He ZZ, Bai L, *et al.* Fe-doped Ni_3S_2/Ni_xP heterojunction with enhanced electron transfer for efficient electrochemical water splitting. J Phys Chem C, 2023, 127: 24583–24590
22 Yang X, Xiao YX, Zhang XQ, *et al.* Enhanced d–π overlap in a graphene supported Ni/PtNi heterojunction for efficient seawater hydrogen evolution. Chem Commun, 2024, 60: 2176–2179
23 Na J, Yu H, Jia S, *et al.* Electrochemical reconstruction of non-noble metal-based heterostructure nanorod arrays electrodes for highly stable anion exchange membrane seawater electrolysis. J Energy Chem, 2024, 91: 370–382
24 Tang J, Liu X, Wang X, *et al.* Unraveling the electron transport propellant mechanism of oxygen vacancy for boosting hydrogen evolution electrocatalysis in alkaline seawater. Small, 2025, 21: 2409675
25 Guo J, Zheng Y, Hu Z, *et al.* Direct seawater electrolysis by adjusting the local reaction environment of a catalyst. Nat Energy, 2023, 8: 264–272
26 Tamura H, Mita K, Tanaka A, *et al.* Mechanism of hydroxylation of metal oxide surfaces. J Colloid Interface Sci, 2001, 243: 202–207
27 Li M, Wang H, Yang Z, *et al.* Synergistic enhancement of alkaline hydrogen evolution reaction by role of Ni-Fe LDH introducing frustrated Lewis pairs via vacancy-engineered. Chin Chem Lett, 2025, 36: 110199
28 Wan C, Zhang Z, Dong J, *et al.* Amorphous nickel hydroxide shell tailors local chemical environment on platinum surface for alkaline hydrogen evolution reaction. Nat Mater, 2023, 22: 1022–1029
29 Le HT, Tran DT, Nguyen TH, *et al.* Single platinum atoms implanted 2D lateral anion-intercalated metal hydroxides of $Ni_2(OH)_2(NO_3)_2$ as efficient catalyst for high-yield water splitting. Appl Catal B-Environ, 2022, 317: 121684
30 Zhang W, Tang Y, Yu L, *et al.* Activating the alkaline hydrogen evo-

lution performance of Mo-incorporated $Ni(OH)_2$ by plasma-induced heterostructure. Appl Catal B-Environ, 2020, 260: 118154
31 Dong Z, Lin F, Yao Y, *et al.* Crystalline $Ni(OH)_2$/amorphous $NiMoO_x$ mixed-catalyst with Pt-like performance for hydrogen production. Adv Energy Mater, 2019, 9: 1902703
32 Shi HY, Chen YX, Ji MH, *et al.* A novel structure Ti/Fe_2O_3/Cu_2S/$Co(OH)_x$ enhances the photoelectrochemical water splitting performance of iron oxide. Chem Synth, 2024, 4: 45
33 Yu J, Wang Q, O'Hare D, *et al.* Preparation of two dimensional layered double hydroxide nanosheets and their applications. Chem Soc Rev, 2017, 46: 5950–5974
34 Long X, Wang Z, Xiao S, *et al.* Transition metal based layered double hydroxides tailored for energy conversion and storage. Mater Today, 2016, 19: 213–226
35 Liu Y, Liu G, Chen X, *et al.* Achieving negatively charged Pt single atoms on amorphous $Ni(OH)_2$ nanosheets with promoted hydrogen absorption in hydrogen evolution. Nano-Micro Lett, 2024, 16: 202
36 Wu YJ, Yang J, Tu TX, *et al.* Evolution of cationic vacancy defects: a motif for surface restructuration of OER precatalyst. Angew Chem Int Ed, 2021, 60: 26829–26836
37 Jang SW, Dutta S, Kumar A, *et al.* Holey Pt nanosheets on NiFe-hydroxide laminates: synergistically enhanced electrocatalytic 2D interface toward hydrogen evolution reaction. ACS Nano, 2020, 14: 10578–10588
38 Hong YR, Dutta S, Jang SW, *et al.* Crystal facet-manipulated 2D Pt nanodendrites to achieve an intimate heterointerface for hydrogen evolution reactions. J Am Chem Soc, 2022, 144: 9033–9043
39 Wang L, Zhang L, Ma W, *et al. In situ* anchoring massive isolated Pt atoms at cationic vacancies of α-$Ni_xFe_{1-x}(OH)_2$ to regulate the electronic structure for overall water splitting. Adv Funct Mater, 2022, 32: 2203342
40 Wang R, Lang J, Liu Y, *et al.* Ultra-small, size-controlled $Ni(OH)_2$ nanoparticles: elucidating the relationship between particle size and electrochemical performance for advanced energy storage devices. NPG Asia Mater, 2015, 7: e183
41 Dai S, Chou JP, Wang KW, *et al.* Platinum-trimer decorated cobalt-palladium core-shell nanocatalyst with promising performance for oxygen reduction reaction. Nat Commun, 2019, 10: 440
42 Shen LW, Wang Y, Shen L, *et al.* Ruthenium nanoparticles decorated with surface hydroxyl and borate species boost overall seawater splitting via increased hydrophilicity. Energy Environ Sci, 2024, 17: 3888–3897
43 Hall DS, Lockwood DJ, Poirier S, *et al.* Raman and infrared spectroscopy of α and β phases of thin nickel hydroxide films electrochemically formed on nickel. J Phys Chem A, 2012, 116: 6771–6784
44 Zhang H, Li P, Chen S, *et al.* Anodic transformation of a core-shell prussian blue analogue to a bifunctional electrocatalyst for water splitting. Adv Funct Mater, 2021, 31: 2106835
45 Subbaraman R, Tripkovic D, Chang KC, *et al.* Trends in activity for the water electrolyser reactions on 3d M(Ni,Co,Fe,Mn) hydr(oxy)oxide catalysts. Nat Mater, 2012, 11: 550–557
46 Han P, Yang X, Wu L, *et al.* A highly-efficient boron interstitially inserted Ru anode catalyst for anion exchange membrane fuel cells. Adv Mater, 2024, 36: 2304496
47 Liu E, Li J, Jiao L, *et al.* Unifying the hydrogen evolution and oxidation reactions kinetics in base by identifying the catalytic roles of hydroxyl-water-cation adducts. J Am Chem Soc, 2019, 141: 3232–3239
48 Gligorovski S, Strekowski R, Barbati S, *et al.* Environmental implications of hydroxyl radicals (·OH). Chem Rev, 2015, 115: 13051–13092
49 Zhang J, Zhang L, Liu J, *et al.* OH spectator at IrMo intermetallic narrowing activity gap between alkaline and acidic hydrogen evolution reaction. Nat Commun, 2022, 13: 5497
50 Shangguan W, Liu Q, Wang Y, *et al.* Molecular-level insight into photocatalytic CO_2 reduction with H_2O over Au nanoparticles by interband transitions. Nat Commun, 2022, 13: 3894
51 Liu B, He D, Ke Z, *et al.* The d-orbital coupling modulation of CuNi alloy for acetonitrile electrochemical reduction and *in-situ* hydrogenation behavior characterization. Sci China Chem, 2023, 66: 3242–3251
52 Xiao YX, Ying J, Chen JB, *et al.* Phosphorous incorporated PtNi networks with synergistic directional electron transfer for efficient and durable seawater hydrogen production. Adv Funct Mater, 2024, 35: 2418264
53 Wei Y, Zhang D, Liu Z, *et al.* Highly efficient catalytic conversion of chloromethane to light olefins over HSAPO-34 as studied by catalytic testing and *in situ* FTIR. J Catal, 2006, 238: 46–57

Acknowledgement This work was supported by the Key R&D Program of Shandong Province, China (2023CXGC010314), National Natural Science Foundation of China (52201286), National 111 Project (B20002), Guangdong Basic and Applied Basic Research Foundation (2024A1515012613, 2025A1515011773, 2025A1515010634), Hubei Provincial Natural Science Foundation of China (2024AFB195), Shenzhen Science and Technology Program (JCYJ20240813103609013), and Fundamental Research Funds for the Central Universities (104972025KFYzxk0014, 104972024KFYjlb0008). We thank the Nanostructure Research Centre (NRC) for performing the S/TEM imaging.

Author contributions Zhao WY performed experiments related to synthesis and electrocatalytic performance. Zhao WY, Yang X, Xiao YX and Yang XY conceived the project, provided the ideas and designed the experiments. Tian G performed TEM and EDX characterizations. Yu F, Tian G, Shen L, Lu Y, Geng W, Wu SM, Ying J, Tiginyanu I and Ozoemena KI provided guidance for materials synthesis. Zhao WY, Yang X, Xiao YX, and Yang XY wrote and revised the paper. All the authors discussed the results, analyzed the data, and gave their approval for submission of the final version of the manuscript.

Conflict of interest The authors declare that they have no conflict of interest.

Supplementary information Supplementary materials are available in the online version of the paper.

Wen-Ying Zhao received her Bachelor degree in materials engineering at the North China University of Water Resources and Electric Power in 2022. She is currently a Master's degree candidate at Wuhan University of Technology, supervised by Prof. Xiao-Yu Yang. Her research interests focus on Pt-based metal compounds for electrocatalysis.

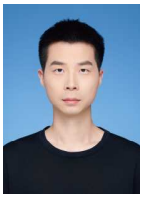

Xiong Yang received his Bachelor degree in materials science at Wuhan University of Technology in 2019. He is currently a PhD candidate under the supervision of Prof. Xiao-Yu Yang at Wuhan University of Technology. His research interest focuses on Pt-based metal compounds in the electrocatalysis field.

Yu-Xuan Xiao received his PhD degree from Wuhan University of Technology in 2021. Currently, he is an associate researcher at Sun Yat-sen University. His research interest focuses on the design and synthesis of metal nanomaterials, as well as their applications in electrocatalysis.

Xiao-Yu Yang earned his BS degree from Jilin University in 2000 and his joint PhD degree from Jilin University, China and Facultes Universitaires Notre-Dame de la Paix (FUNDP), Belgium (co-education) in 2007. After a post-doctoral fellowship at the FUNDP, he worked as a "Chargé de Recherches" at the Fondation Nationale de la Recherche Scientifique (F.N.R.S.) of Belgium. He is currently working as a full professor at the State Key Laboratory of Advanced Technology for Material Synthesis and Processing and a visiting professor at Harvard University.

富羟基PtNi纳米粒子作为海水中电化学析氢反应的高效催化剂

赵文英[1†], 杨雄[1†], 肖宇轩[2*], 余菲[1], 田歌[1], 沈凌[1], 卢毅[1], 耿伟[1], 吴思明[1], 应杰[2], Ion Tiginyanu[3], Kenneth I. Ozoemena[4], 阳晓宇[1,5*]

摘要 Cl^-吸附及腐蚀效应是Pt基催化剂在海水析氢反应(HER)中性能的主要障碍. 虽然引入羟基是提升HER动力学和缓解氯毒化的有效策略, 但在Pt基催化剂体系中实现这一策略仍具挑战性. 本研究通过高温还原法制备了具有Ni空位(路易斯酸位点)的PtNi合金纳米颗粒. 路易斯酸位点促进Ni-LDH载体上晶格羟基向表面羟基的转化. Ni-LDH的晶格羟基通过与路易斯酸位点相互作用, 产生表面羟基并协同提升其表面亲水性. 这种双功能特性既能促进水分子吸附, 又可抑制Cl^-吸附. 优化后的PtNi/Ni-LDH在碱性真实海水中展现出优异的HER性能, 仅需19 mV过电位即可达到10 mA cm^{-2}电流密度, 塔菲尔斜率为31 mV dec^{-1}, 并在100小时耐久性测试中具有优异的稳定性. 该研究为通过定向羟基工程设计高效海水裂解催化剂提供了理论基础.